大韓土木學會論文集
第12卷 第3號 · 1992年 9月
pp. 25~37

構 造 工 學

# 변화되는 재료의 기준 물성치에 근거한 매우 큰 변화에 대한 비선형 유한요소의 정식화

# A Nonlinear Finite Element Formulation for Very Large Deformation based on Updated Material Reference Frame

윤영묵* · 박문호**
Yun, Young Muk · Park, Moon Ho

요 지

매우 큰 기하학적 변화를 나타낼 수 있는 비선형 유한요소의 정식화 과정을 나타내었다. 유한요소의 구성은 변화되는 재료의 기준 물성치에 근거를 두고 형성하였으므로 매우 큰 변형을 받는 재료의 특성들을 진응력 · 변형율 시험에 정확히 직접 적용할 수 있도록 하였다. 큰 변형 문제에 대하여 연속체 역학적인 접근방법으로 일관된 공식을 유도하였다. 운동학적인 문제는 변화되는 재료의 물성 기준치가 더욱 더 요구되므로, 물체 평형 방정식을 변화되는 기하학적 좌표로서 또한 형성하였으며, 이에 2차 Piola-Kirchhoff 응력과 변화되는 Largrangian 변형을 텐서들이 사용되었다. 수치해는 명확한 증분적인 수치과정으로 유도하였으며, 수치해의 증명을 위하여 뼈대구조와 평면구조들의 매우 큰 변형에 대한 예제들을 해석하였다. 또한 적절히 취급되는 재료 특성에 대한 중요성을 논증하였다.

Abstract

A nonlinear finite element formulation which has the capability of handling very large geometrical changes is presented. The formulation is based on an updated material reference frame and hence true stress-strain test can be directly applied to properly characterize properties of materials which are subjected to very large deformation. For the large deformation, a consistent formulation based on the continuum mechanics approach is derived. The kinematics is referred to an updated material frame. Body equilibrium is also established in an updated geometry and the second Piola-Kirchhoff stress and the updated Lagrangian strain tensor are used in the formulation.

Numerical examples for very large deformation of framed structures and plane solids are analyzed for verification purposes. The numerical solutions are obtained by an incremental numerical procedure. The importance of handing material properties properly is also demonstrated.

* 미국 퍼듀대학교 토목공학과 박사과정수료 · 연구조교
** 정회원 · 경북대학교 공과대학 토목공학과 교수

## 1. Introduction

In recent years, behaviors of structures subjected to large deformation have been the subjects of considerable research. For a realistic prediction of such behaviors, both geometric and material nonlinearities should be considered. Different formulations and procedures to accommodate the nonlinear behaviors of large deformation have been suggested[1-15]. Among them, two types of Lagrangian formulations have been widely used in the finite element applications.

The first type is the Total Lagrangian Formulation(TLF) where the deformation of a body is measured from its own initial reference frame. Any subsequent deformation of the body is also referred to the initial material frame. The use of TLF is appealing because of the simplicity with which material rates of changes can be calculated. Another advantage arises in the treatment of boundary conditions on the surface of the body which is changing during its deformation. Since the formulation refers the motion and force to a fixed reference configuration, it enables one to treat the coupling with the geometrical changes in a relatively simple manner. The disadvantages of the formulation stem from the requirements that the adopt a mathematical consistent state of stresses and stress rates acting on the current configuration, the reference to the initial reference configuration leads to a formulation which is physically artificial, and hence it becomes difficult to evaluate material parameters. Another difficulty is the numerical handling of the excessive deformations of a structure subjected to very large deformation changes may cause a great deal of distortion in the original finite element mesh, and such distortions may greatly affect the accuracy and the stability of the solution procedure.

The second type is the Updated Lagrangial Formulation(ULF) where the current configuration of the body is taken as the reference for the variational formulation although the basic kinematics of the continuum is still based on a fixed material frame. Owing to the nature of each formulation and its reference configuration, this formulation has some advantages over TLF. For example, the boundary condition updation and mesh distortion seem to be easier to handle and the choice of the current configuration as the reference for the variational formulation may result in neglecting nonlinear terms of kinematic variables.

Most of the current large deformation algorithms show serious numerical limitations. Typically, the solutions become unstable at a certain point either when the iterations fail to converge or the algorithms fail to handle the negative deformation gradient when the deformation becomes very large. A more serious problem common to all formulations is that the definitions of stress and strain, their increments and constitutive equations include the geometrical couplings, and hence correlating them to the material testing data become difficult.

The objective of this paper is to derive a nonlinear finite element formulation which has the capability of (a) handling very large geometrical changes without the need for lengthy iterations and (b) handling the material data more accurately. The formulation is based on an updated material reference frame and true stress-strain data are proposed to characterize material properties.

## 2. Continuum formulation

Consider the motion of a body in a Cartesian rectangular coordinate system as shown Figure 2.1 where the body is subjected to large configurational changes due to external loadings. To employ an incremental formulation, a time variable is used to conveniently describe the load increment and the corresponding motions.

In figure 2.1, three configurations are considered: the initial configuration $C_0$ at time 0, current configuration $C_1$ at time $t$, and neighborhood configuration $C_2$ at time $t+\Delta t$, respectively. The position vectors of a particle $P$ and the coordinates describing the configuration of the body are, respectively, ${}^{i}\underline{X}$ and ${}^{i}\underline{X}_k$, where left superscript $i(=0, 1, 2)$ refers to the configuration of the body and right subscript $k(1, 2, 3)$ refers to the coordinate axes. During the motion, the volume, the surface

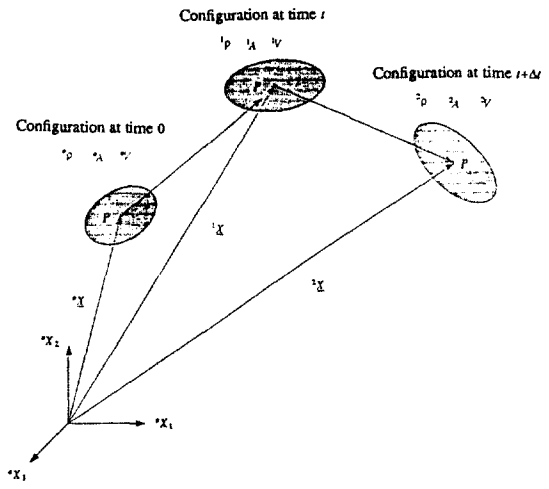


Figure 2.1. Motion of body in stationary Cartesian coordinate system.

area, and the mass density of the body change continuously. The specific mass, surface area, and volume of the body in each configuration are denoted ${}_{t}\rho$, ${}^{t}A$, and ${}^{t}V$, respectively.

We consider that the solutions at times 0, $\Delta t$, $2\Delta t$, $\cdots$, and $t$ are known, where $\Delta t$ is a time increment. It is required to solve for the unknown variable at time $t+\Delta t$. Considering the equilibrium of the body in the configuration $C_2$, the principle of virtural displacements gives

$$\delta\,{}^{2}U-\delta\,{}^{2}W=0 \tag{2.1}$$

where $\delta\,{}^{2}U$ and $\delta\,{}^{2}W$ are, respectively, the internal and external virtual works in the configuration at time $t+\Delta t$:

$$\delta\,{}^{2}U=\int_{{}_{0}V} tr({}^{2}_{0}\underline{S}\;\delta^{2}_{0}\underline{E})\,d^{0}V \tag{2.2}$$

$$\delta\,{}^{2}W=\int_{{}^{2}A}(\delta^{2}_{0}\underline{u})^{T}\,{}^{2}\underline{T}\,d^{2}A+\int_{{}^{2}V}(\delta^{2}_{0}\underline{u})^{T}\,{}^{2}\rho\,{}^{2}\underline{b}\,d^{2}V \tag{2.3}$$

In eqn (2.2), ${}^{2}_{0}\underline{S}$ and $\delta^{2}_{0}\underline{E}$ are, respectively, the second Piola-Kirchhoff stress tensor and the variation of Green-Lagrange strain tensor which are measured in the configuration $C_2$ but referred to the initial configuration and $tr({}^{2}_{0}\underline{S}\;\delta^{2}_{0}\underline{E})$ stands for the *trace* of a second-order tensor $({}^{2}_{0}\underline{S}\;\delta^{2}_{0}\underline{E})$ which is a scalar invariant function of the tensor, having the same numerical value in all coordinate systems. In what follows, left superscripts indicate the configuration at which the quantity is measured whereas left subscripts indicate the relative configuraton to which the quantity is referred. In eqn (2.3), $(\delta^{2}_{0}\underline{u})^{T}$ is the transpose of virtual displacement vector and ${}^{2}\underline{T}$ and ${}^{2}\underline{T}$ and ${}_{2}\underline{b}$ are, respectively, the surface traction and body force vectors which are applied in the configuration $C_2$ which is in equilibrium state:

$${}^{2}\underline{T}={}^{2}\underline{T}_{m}+\Delta^{2}\underline{T} \tag{2.4}$$

$${}^{2}\underline{b}={}^{2}\underline{b}_{m}+\Delta^{2}\underline{b} \tag{2.5}$$

where ${}^{2}\underline{T}_{m}$ and ${}^{2}\underline{b}_{m}$ are, respectively, the surface traction and body force vectors which are applied initially in the current configuration but adjusted by the changes of surface area, mass density, and volume and applied in the configuration $C_2$ and $\Delta^{2}\underline{T}$ and $\Delta^{2}\underline{b}$ are, respectively, the incremental surface traction and body force vectors which are applied in the configuration $C_2$.

Considering the current configuration of the body as a material and geometry reference frame, the internal and external virtual works in the configuration $C_2$ are given by

$$\delta\,{}^{2}U=\int_{{}_{1}V} tr({}^{2}_{1}\underline{S}\;\delta^{2}_{1}\underline{E})\,d^{1}V \tag{2.2}$$

$$\delta\,{}^{2}W=\int_{{}_{2}A}(\delta^{2}_{1}\underline{u})^{T}\,{}^{2}\underline{T}\,d^{2}A+\int_{{}_{2}V}(\delta^{2}_{1}\underline{u})^{T}\,{}^{2}\rho\,{}^{2}\underline{b}\,d^{2}V \tag{2.7}$$

where

$${}^{2}_{1}\underline{S}=\frac{{}^{1}\rho}{{}^{2}\rho}({}^{2}_{1}\underline{F})^{-1}\,{}^{2}\underline{\sigma}\,({}^{2}_{1}\underline{F})^{-T}={}^{1}\underline{\sigma}+\Delta^{2}_{1}\underline{S} \tag{2.8}$$

$${}^{2}_{1}\underline{E}=\frac{1}{2}[({}^{2}_{1}\underline{F})^{T}\,{}^{2}_{1}\underline{F}-\underline{I}]={}^{2}_{1}\underline{e}+{}^{2}_{1}\underline{\eta} \tag{2.9}$$

In eqns (2.8) and (2.9), ${}^{1}\underline{\sigma}$ and ${}^{2}\underline{\sigma}$ are, respectively, Cauchy stress tensors in the configurations $C_1$ and $C_2$, $\Delta^{2}_{1}\underline{S}$ is the incremental second Piola-Kirchhoff stress tensor, $\underline{I}$ is the identity tensor, and ${}^{2}_{1}\underline{F}$, ${}^{2}_{1}\underline{e}$, and ${}^{2}_{1}\underline{\eta}$ are, respectively, the deformation and linear and nonlinear parts of Green-Lagrange strain tensor.

By the analogous procedures to the derivation of the eqns (2.6) and (2.7), the internal and exter-

nal virtual works in the current configuration are given by

$$\delta\,{}^1U=\int_{{}^1V}\frac{{}^1\rho}{{}^t\rho}\,tr({}^1_t\underline{S}\,\delta{}^1_t\underline{E})\,d^1V \tag{2.10}$$

$$\delta\,{}^1W=\int_{{}^1A}(\delta{}^1_t\underline{u})^T\,{}^1\underline{T}\,d^1A+\int_{{}^1V}(\delta{}^1_t\underline{u})^T\,{}^1\rho\,{}^1\underline{b}\,d^1V \tag{2.11}$$

where ${}^t\rho$ is the mass density in the configuration at time $t-\Delta t$, $(\delta{}^1_t\underline{u})^T$ is the transpose of virtual displacement vector in the current configuration ${}^1_t\underline{S}$ and ${}^1_t\underline{E}$ are, respectively, the second Piola-Kirchhoff stress and Green-Lagrange strain tensors which are measured in the current configuration but referred to the configuration at time $t-\Delta t$, and ${}^1\underline{T}$ and ${}^1\underline{b}$ are, respectively, the surface traction and body force vector which are applied in the current configuration.

Since the deformation gradient tensor is, in general, considered as the same as the identity tensor for small increments, i.e., ${}^1_t\underline{F}=\partial{}^1\underline{X}/\partial{}^t\underline{X}\approx\underline{I}$, the ratio of mass densities $\frac{{}^1\rho}{{}^t\rho}$ and the second Piola-Kirchhoff stress tensor ${}^1_t\underline{S}$ become

$$\frac{{}^1\rho}{{}^t\rho}=\frac{1}{det|{}^1_t\underline{F}|}\approx 1,\quad {}^1_t\underline{S}=\frac{{}^t\rho}{{}^1\rho}({}^1_t\underline{F})^{-1}\,{}^1\underline{\sigma}({}^1_t\underline{F})^{-T}\approx{}^1\underline{\sigma} \tag{2.12}$$

Also, the virtual displacement vector and the variation of Green-Lagrangian tensor in the configurations $C_1$ and $C_2$ maybe approximated by $\delta{}^2_1\underline{u}\approx\delta{}^1_t\underline{u}$ and $\delta{}^2_1\underline{E}\approx\delta{}^1_t\underline{E}$ for small increments. Hence, considering the approximations, the internal, the internal and external virtual works are given by

$$\delta\,{}^1U=\int_{{}^1V}tr({}^1\underline{\sigma}\delta{}^2_1\underline{E})\,d^1V \tag{2.13}$$

$$\delta\,{}^1W=\int_{{}^1A}(\delta{}^2_1\underline{u})^T\,{}^1\underline{T}\,d^1A+\int_{{}^1V}(\delta{}^2_1\underline{u})^T\,{}^1\rho\,{}^1\underline{b}\,d^1V \tag{2.14}$$

Note that theCauchy stresses in eqn (2.13) are physically the same as the second Piola-Kirchhoff stresses if the current configuration is used as a reference frame.

Subtacting equns (2.13) and (2.14) from eqns (2.6) and (2.7), respectively, and considering equns (2.4), (2.5), and (2.8), the incremental internal and external virtual works are obtained by

$$\delta(\Delta U)=\delta\,{}^2U-\delta\,{}^1U=\int_{{}^1V}tr(\Delta{}^2_1\underline{S}\,\delta{}^2_1\underline{E})\,d^1V \tag{2.15}$$

$$\delta(\Delta W)=\delta\,{}^2W-\delta\,{}^1W=\int_{{}^2A}(\delta{}^2_1\underline{u})^T\,({}^2\underline{T}_m+\Delta{}^2\underline{T})\,d^2A-\int_{{}^1A}(\delta{}^2_1\underline{u})^T\,{}^1\underline{T}\,d^1A+\int_{{}^2V}(\delta{}^2_1\underline{u})^T\,{}^2\rho({}^2\underline{b}_m+\Delta{}^2\underline{b})\,d^2V-\int_{{}^1V}{}^1\rho(\delta{}^2_1\underline{u})^T\,{}^1\underline{b}\,d^1V \tag{2.16}$$

Considering the external forces which maintain the same direction and magnitude, i.e.,

$${}^2\underline{T}_m\,d^2A={}^1\underline{T}\,d^1A,\quad \Delta{}^2\underline{T}\,d^2A=\Delta\underline{T}\,d^1A \tag{2.17a}$$

$${}^2\rho{}^2\underline{b}_m\,d^2V={}^1\rho{}^1\underline{b}\,d^1V,\quad {}^2\rho\,\Delta{}^2\underline{b}\,d^2V={}^1\rho\,\Delta\underline{b}\,d^1V \tag{2.17b}$$

the incremental external virtual work, eqn (2.16), becomes

$$\delta(\Delta W)=\int_{{}^1A}(\delta{}^2_1\underline{u})^T\,\Delta\underline{T}\,d^1A+\int_{{}^1V}(\delta{}^2_1\underline{u})^T\,{}^1\rho\,\Delta\underline{b}\,d^1V \tag{2.18}$$

where $\Delta\underline{T}$ and $\Delta\underline{b}$ are, respectively, incremental surface and body force vectors which are applied initially in the configuration $C_2$ but adjusted and applied in the current configuration.

By equating eqns (2.15) with linear part of Green-Lagrange strain and (2.18), equation for the motion of a body is given by

$$\int_{{}^1V}tr(\Delta{}^2_1\underline{S}\,\delta{}^2_1\underline{e})\,d^1V=\int_{{}^1A}(\delta{}^2_1\underline{u})^T\,\Delta\underline{T}\,d^1A+\int_{{}^1V}(\delta{}^2_1\underline{u})^T\,{}^1\rho\,\Delta\underline{b}\,d^1V \tag{2.19}$$

where $\Delta{}^2_1\underline{S}={}^t\underline{C}\,{}^2_1\underline{e}$ and ${}^t\underline{C}$ is the updated constant elasticity tensor relating small strain increments to the corresponding stress increments.

## 3. Discrete formulation

For the isoparmetric element solution, the coordinates and displacements in the current configuration are, respectively, interpolated as

$${}^1X_i=\sum_{k=1}^{n}N_k\,{}^1X_i^k \tag{3.1}$$

$${}^2_1u_i=\sum_{k=1}^{n}N_k\,{}^2_1u_i^k \tag{3.2}$$

where ${}^1X_i^k$ and ${}^2_1u_i^k$ are, respectively, the coordinate and the nodal displacement of nodalpoint $k$, $N_k$ is the interpolation function corresponding to no-

dal point $k$, and $n$ is the number of element nodal points.

Substituting the element coordinate and displacement interpolations into eqn (2.19), we obtain, for a single element

$$ {}^{1}\underline{K}\,{}^{2}_{1}\underline{u} = \Delta^{1}\underline{R} \tag{3.3} $$

where ${}^{1}\underline{K}$ and $\Delta^{1}\underline{R}$ are, respectively, the stiffness matrix and the incremental element nodal force vector, and ${}^{2}_{1}\underline{u}$ is the element nodal displacement vector in the configuration $C_2$ referred to the current configuration. The basic integrals considered and the corresponding matrix evaluations are obtained by

$$ \delta(\Delta U) = \int_{{}^{1}V} tr({}^{t}\underline{C}\,{}^{2}_{1}\underline{e}\;\delta\,{}^{2}_{1}\underline{e})\, d^{1}V \tag{3.4a} $$

$$ {}^{1}\underline{K}\,{}^{2}_{1}\underline{u} = \left(\int_{{}^{1}V} {}^{1}\underline{B}^{T}\,{}^{t}\underline{C}\,{}^{1}\underline{B}\, d^{1}V\right) {}^{2}_{1}\underline{u} \tag{3.4b} $$

$$ \delta(\Delta W) = \int_{{}^{1}A} (\delta\,{}^{2}_{1}\underline{u})^{T}\,\Delta\underline{T}\, d^{1}A + \int_{{}^{1}V} (\delta\,{}^{2}_{1}\underline{u})^{T}\,{}^{1}\rho\,\Delta\underline{b}\, d^{1}V \tag{3.5a} $$

$$ \Delta^{1}\underline{R} = \int_{{}^{1}A} \underline{N}^{T}\,\Delta\underline{T}\, d^{1}A + \int_{{}^{1}V} \underline{N}^{T}\,{}^{1}\rho\,\Delta\underline{b}\, d^{1}V \tag{3.5b} $$

where ${}^{1}\underline{B}$ and $\underline{N}^{T}$ are the linear strain-displacement transformation matrix and the transpose of displacement interpolation matrix, respectively, and ${}^{t}\underline{C}$ is the updated constant elasticity tensor. In the analysis of framed structures ${}^{t}E$(eqn 4.21) is used as a part of ${}^{t}\underline{C}$, whereas in the analysis of plane solids ${}^{t}E$ and ${}^{t}\nu$ are used to form the updated constant elasticity tensor ${}^{t}\underline{C}$ in the current configuration. Note that the elements of matrices in eqns (3.4b) and (3.5b) are functions of the natural element coordinates and that the volume and area integrations are performed using a coordinate change from Cartesian to natural coordinates.

## 4. Material properties

An important aspect of the analysis for large deformation is the proper characterization of material properties. Since the second Piola-Kirchhoff stress is not a physical quantity and the increment of Cauchy stress does not satisfy objectivity requirement, existing large deformation algorithms based on the use of initial configuration as a material reference frame are known to have difficulties in material modeling. By using the current configuration as a reference frame, material models for ture stress-strain response can be conveniently implemented even for structures subjected to very large geometrical changes.

For the purpose of numerical verification, the material constants based on current configuration and those based on initial configuration must be correlated. These can be obtained by considering large deformation of a rod due to axial tension.

Consider a three dimensional rod subjected to axial forces with length ${}^{o}l$ and cross sectional area ${}^{o}A$ in the initial configuration, as shown in Figure 4.1(a). The deformation gradient and second Piola-Kirchhoff stress tensors in the current configuration are given by

$$ {}^{1}_{o}\underline{F} = \frac{\partial\,{}^{1}\underline{x}}{\partial\,{}^{p}\underline{x}}\;\frac{\partial\,{}^{p}\underline{x}}{\partial\,{}^{o}\underline{x}} = {}^{1}_{p}\underline{F}\;{}^{p}_{o}\underline{F} \tag{4.1} $$

$$ {}^{1}_{o}\underline{S} = {}^{p}_{o}\underline{S} + {}^{o}\underline{C}\;{}^{1}_{p}\underline{E} \tag{4.2} $$

where

$$ {}^{p}_{o}\underline{F} = \begin{bmatrix} {}^{p}_{o}\lambda_1 & 0 & 0 \\ 0 & {}^{p}_{o}\lambda_2 & 0 \\ 0 & 0 & {}^{p}_{o}\lambda_2 \end{bmatrix},\quad {}^{1}_{p}\underline{F} = \begin{bmatrix} {}^{1}_{p}\lambda_1 & 0 & 0 \\ 0 & {}^{1}_{p}\lambda_1 & 0 \\ 0 & 0 & {}^{1}_{p}\lambda_2 \end{bmatrix} \tag{4.3} $$

$$ {}^{1}_{p}\underline{E} = \frac{1}{2}\begin{bmatrix} ({}^{1}_{p}\lambda_2)^2 - 1 & 0 & 0 \\ 0 & ({}^{1}_{p}\lambda_2)^2 - 1 & 0 \\ 0 & 0 & ({}^{1}_{p}\lambda_2)^2 - 1 \end{bmatrix} \tag{4.4} $$

In the above equations, ${}^{1}_{p}\lambda_1$, ${}^{1}_{p}\lambda_2$ and ${}^{p}_{o}\lambda_1$, ${}^{p}_{o}\lambda_2$ are, respectively, the components of the deformation gradient tensor ${}^{1}_{p}\underline{F}$ and ${}^{p}_{o}\underline{F}$ which are measured in the configurations at time $t$ and $t-\Delta t$ but referred to the configurations at time $t-\Delta t$ and 0, respectively, and ${}^{o}\underline{C}$ is the constant elasticity tensor in the initial configuration. Since theCauchy stresses in the current configuration may be expressed in terms of the second Piola-Kirchhoff stresses, along the principle axes they are given, using indicial notation, by

$$ {}^{1}\sigma_{ii} = \frac{{}^{1}\rho}{{}^{o}\rho}({}^{1}_{o}F_{ii})^{2}\,{}^{1}_{o}S_{ii},\quad i = 1,\ 2,\ 3 \tag{4.5} $$

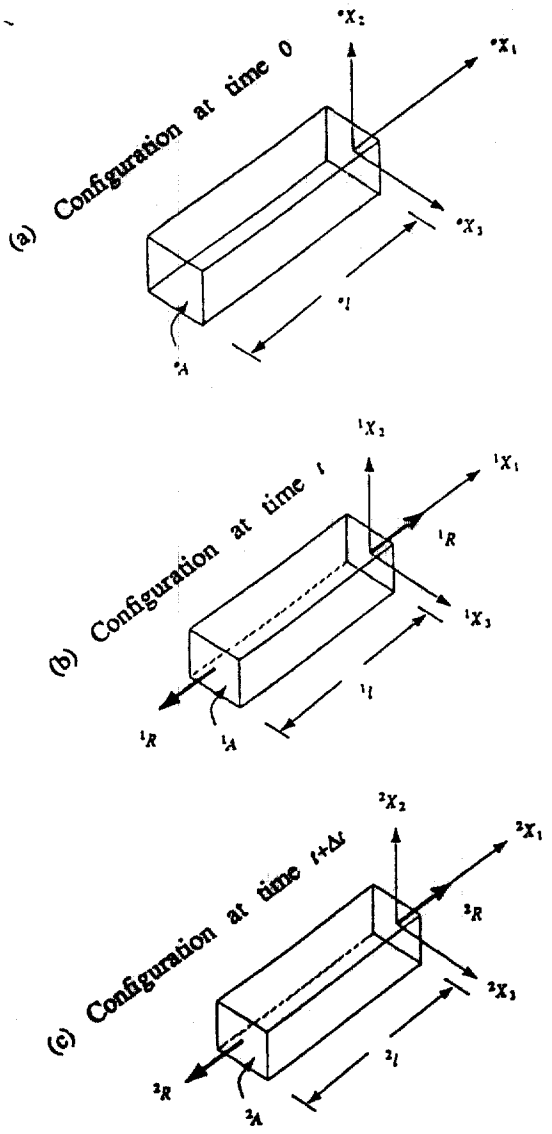


Figure 4.1. Three-dimensional rod element with its local coordinates

where ${}^{t}_{0}S_{ii}$ are the components of the second Piola-Kirchhoff stress tensor:

$$ {}^{1}_{0}S_{ii}={}^{t}_{0}S_{ii}+\frac{1}{2}[[{}^{0}C_{i111}[{}^{t}_{0}\lambda_1)^2-1] +({}^{0}C_{i122}+{}^{0}C_{i133})[({}^{t}_{0}\lambda_2)^2-1]] \tag{4.6} $$

where ${}^{0}C_{i111}$, ${}^{0}C_{i122}$, and ${}^{0}C_{i133}$ are components of the constant elasticity tensor ${}^{0}\underline{C}$.

Introducing the force condition and assuming isotropy in the current configuration, i.e.,

$$ {}^{1}R={}^{1}\sigma_{11}\,{}^{1}A,\ {}^{1}\sigma_{22}={}^{1}\sigma_{33}=0 \tag{4.7} $$

the expression of the applied force in the current configuration is obtained by

$$ {}^{1}R=\frac{{}^{1}\rho}{{}^{0}\rho}({}^{1}_{0}F_{11})^2\,[{}^{t}_{0}S_{11}+\frac{1}{2}[{}^{0}C_{1111}[({}^{t}_{0}\lambda_1)^2-1] +({}^{0}C_{1122}+{}^{0}C_{1133})[({}^{t}_{0}\lambda_2)^2-1]]]\,{}^{1}A \tag{4.8} $$

where

$$ ({}^{t}_{0}\lambda_2)^2-1=-\frac{2{}^{t}_{0}S_{22}}{{}^{0}C_{2222}+{}^{0}C_{2233}}-{}^{0}\nu[({}^{t}_{0}\lambda_1)^2-1] \tag{4.9} $$

In eqn (4.9), ${}^{0}\nu$ is the Poisson's ratio in the initial configuration.

By an analogous procedure to the derivation of the eqns (4.8) and (4.9), the expression of the applied force in the configuration $C_2$ is obtained by

$$ {}^{2}R={}^{2}\sigma_{11}\,{}^{2}A=\frac{{}^{2}\rho}{{}^{1}\rho}({}^{2}_{0}F_{11})^2\,[{}^{1}_{0}S_{11}+\frac{1}{2}[{}^{0}C_{1111}[({}^{2}_{1}\lambda_1)^2 -1]+({}^{0}C_{1122}+{}^{0}C_{1133})[({}^{2}_{1}\lambda_2)^2-1]]] det|{}^{2}_{1}\underline{F}|({}^{2}_{1}F_{11})^{-1}\,{}^{1}A \tag{4.10} $$

where

$$ {}^{2}_{0}\underline{F}={}^{2}_{1}\underline{F}\,{}^{1}_{0}\underline{F}=\begin{bmatrix} {}^{2}_{1}\lambda_1 & 0 & 0 \\ 0 & {}^{2}_{1}\lambda_2 & 0 \\ 0 & 0 & {}^{2}_{1}\lambda_2 \end{bmatrix}\begin{bmatrix} {}^{1}_{0}\lambda_2 & 0 & 0 \\ 0 & {}^{1}_{0}\lambda_1 & 0 \\ 0 & 0 & {}^{1}_{0}\lambda_2 \end{bmatrix} $$

$$ ({}^{2}_{1}\lambda_2)^2-1=-\frac{2{}^{1}_{0}S_{22}}{{}^{0}C_{2222}+{}^{0}C_{2233}}-{}^{0}V[({}^{2}_{1}\lambda_1)^2-1] \tag{4.12} $$

Subtracting eqn (4.8) from eqn (4.10), the expression of the incremental applied force $\Delta R$ is given by

$$ \Delta R=\frac{{}^{2}\rho}{{}^{0}\rho}({}^{2}_{0}F_{11})^2\,{}^{2}_{0}S_{11}\,det|{}^{2}_{1}\underline{F}|({}^{2}_{1}F_{11})^{-1}\,{}^{1}A -\frac{{}^{1}\rho}{{}^{0}\rho}({}^{1}_{0}F_{11})^2\,{}^{1}_{0}S_{11}\,{}^{1}A \tag{4.13} $$

where

$$ {}^{1}_{0}S_{11}={}^{t}_{0}S_{11}+\frac{1}{2}[{}^{0}E[({}^{t}_{0}\lambda_1)^2-1]-4{}^{0}\nu{}^{t}_{0}S_{22}] $$

$$ {}^{2}_{0}S_{11}={}^{1}_{0}S_{11}+\frac{1}{2}[{}^{0}E[({}^{2}_{1}\lambda_1)^2-1]-4{}^{0}\nu{}^{1}_{0}S_{22}] $$

In the above equation, ${}^{o}E$ is the Young's modulus of elasticity inthe current configuration.

Now, based on the current configuration as the material reference frame, the incremental second Piola-Kirchhoff stresses ${}^{2}_{1}S_{ij}$, incremental Cauchy stresses ${}^{2}_{1}\sigma_{ij}$, and incremental applied force $\Delta R$ may be found. Using the relationship of the second Piola-Kirchhoff stress and Cauchy stress, we obtain the increment of Cauchy stresses along the principle axes by

$$\Delta^{2}_{1}\sigma_{ii}=\frac{{}^{2}\rho}{{}^{1}\rho}({}^{2}_{1}F_{ii})^{2}\,\Delta^{2}_{1}S_{ii},\ i=1,\ 2,\ 3 \tag{4.14}$$

where

$$\Delta^{2}_{1}S_{ii}={}^{t}C_{iirs}\,{}^{2}_{1}E_{rs}=\frac{1}{2}\,[[{}^{t}C_{ii11}({}^{2}_{1}\lambda_{1})^{2}-1]\times({}^{t}C_{ii22}+{}^{t}C_{ii33})[({}^{2}_{1}\lambda_{2})^{2}-1]] \tag{4.15}$$

${}^{t}C_{ii11}$, ${}^{t}C_{ii22}$, and ${}^{t}C_{ii33}$ in the above equation are components of the constant elasticity tensor, ${}^{t}\underline{C}$, of the current configuration.

Assume that the stress-strain relationships in the current configuration is linear and isotropic,i. e.,

$${}^{t}C_{1111}=\frac{{}^{t}E(1-{}^{t}\nu)}{(1+{}^{t}\nu)(1-2{}^{t}\nu)}={}^{t}C_{2222}={}^{t}C_{3333} \tag{4.16a}$$

$${}^{t}C_{1122}=\frac{{}^{t}\nu}{1-{}^{t}\nu}\,{}^{t}C_{1111}={}^{t}C_{1133}={}^{t}C_{2233},\ \textit{symmetric} \tag{4.16b}$$

Since the incremental Cauchy stresses are zero along the lateral principle axes, with the substitution of the relationships given in eqn (4.16) into eqn (4.14) an solving for ${}^{t}\nu$, we have

$${}^{t}\nu=\frac{1-({}^{2}_{1}\lambda_{2})^{2}}{({}^{2}_{1}\lambda_{1})^{2}-1} \tag{4.17}$$

where ${}^{t}\nu$ is the updated Poisson's ratio in the current configuration. We also evaluate the incremental applied force $\Delta R$ by

$$\Delta R=\Delta^{2}_{1}\sigma_{11}\,{}^{2}A=\frac{1}{2}\,\frac{{}^{2}\rho}{{}^{1}\rho}({}^{2}_{1}F_{11})^{2}[{}^{t}C_{1111}[({}^{2}_{1}\lambda_{1})^{2}-1]+({}^{t}C_{1122}+{}^{t}C_{1133})[({}^{2}_{1}\lambda_{2})^{2}-1]]\ det|{}^{2}_{1}\underline{F}|({}^{2}_{1}F_{11})^{-1}\,{}^{1}A \tag{4.18}$$

Substituting the relation

$$\frac{{}^{2}\rho}{{}^{1}\rho}=\frac{1}{det|{}^{2}_{1}\underline{F}|}=\frac{1}{{}^{2}_{1}\lambda_{1}({}^{2}_{1}\lambda_{2})^{2}} \tag{4.19}$$

and the stress-strain relationships given in eqn (4.16) into eqn (4.18), we have

$$\Delta R=\frac{{}^{2}_{1}\lambda_{1}}{2({}^{2}_{1}\lambda_{2})^{2}}\,{}^{t}E[({}^{2}_{1}\lambda_{1})_{2}-1]\ det|{}^{2}_{1}\underline{F}|({}^{2}_{1}F_{11})^{-1}\,{}^{1}A \tag{4.20}$$

where ${}^{t}E$ is the updated Young's modulus of elasiticity in the current configuration.

By equating eqns (4.13) and (4.20) and solving for ${}^{t}E$, we have

$${}^{t}E=\frac{2({}^{2}_{1}\lambda_{2})^{2}}{{}^{2}_{1}\lambda_{1}[({}^{2}_{1}\lambda_{1})^{2}-1}\left[\frac{{}^{2}\rho}{{}^{o}\rho}({}^{2}_{o}F_{11})^{2}\,{}^{2}_{o}S_{11}-\frac{{}^{1}\rho}{{}^{o}\rho}\,\frac{({}^{1}_{o}F_{11})^{2}}{det|{}^{2}_{1}\underline{F}|({}^{2}_{1}F_{11})^{-1}}\,{}^{1}_{o}S_{11}\right] \tag{4.21}$$

## 5. Numerical Examples

To validate the presented formulation and demonstrate the importance of imposing material properties properly, four examples are given.

For the analysis of framed structures, the element equations are formulated in the body attached coordinate as shown in Figure 5.1 and then transformed to the global coordinate. The axes of the frame member are assumed to be the linear interpolation for the axial displacement and cubic interpolation for bending displacement in the body attached coordinates. The axial and bending displacements of the frame element along the body attached coordinates in the configuration at time $t$ are given by

$${}^{2}_{1}\hat{u}=\underline{N}_{r}^{T}\,{}^{2}_{1}\hat{\underline{u}}_{r},\ {}^{2}_{1}\hat{v}=\underline{N}_{b}^{T}\,{}^{2}_{1}\hat{\underline{u}}_{b} \tag{5.1}$$

where $\underline{N}_{r}$ and $\underline{N}_{b}$ are, respectively, the vectors of interpolation functions for a rod and a beam element with two nodes and ${}^{2}_{1}\hat{\underline{u}}_{r}$ and ${}^{2}_{1}\hat{\underline{u}}_{b}$ are, respectively, the vectors of axial and bending displacements:

$$\underline{N}_{r}=[N_{r1}\,N_{r2}]^{T},\ \underline{N}_{b}=[N_{b1}\,N_{b2}\,N_{b3}\,N_{b4}]^{T} \tag{5.2}$$

$${}^{2}_{1}\hat{\underline{u}}_{r}=[\hat{u}_{1}\ \hat{u}_{2}]^{T},\ {}^{2}_{1}\hat{\underline{u}}_{b}=[\hat{v}_{1}\ \hat{\theta}_{1}\ \hat{v}_{2}\ \hat{\theta}_{2}]^{T} \tag{5.3}$$

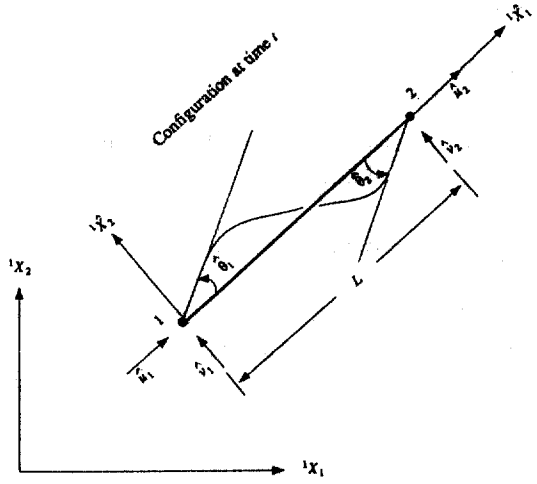


Figure 5.1. Frame element with body attached coordinates in the configuration at time $t$.

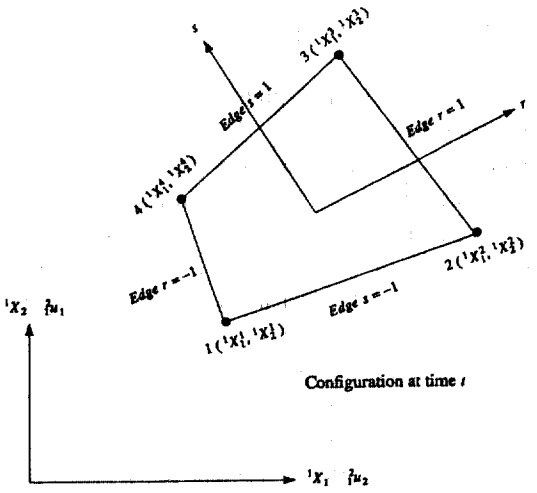


Figure 5.2. Four-node plane solid element in the configuration at time $t$.

In eqn (5.2), the interpolation functions for a rod and a beam element are given by

$$N_{r1}=1-\frac{{}^1\hat{x}_1}{L},\quad N_{r2}=\frac{{}^1\hat{x}_1}{L} \tag{5.4a}$$

$$N_{b1}=\frac{1}{L^3}[2({}^1\hat{x}_1)^3-3({}^1\hat{x}_1)^2L+L^3],$$

$$N_{b2}=\frac{1}{L^3}[({}^1\hat{x}_1)^3L-2({}^1\hat{x}_1)^2L+{}^1\hat{x}_1L^3],$$

$$N_{b3}=\frac{1}{L^3}[-({}^1\hat{x}_1)^3+3({}^1\hat{x}_1)^2],$$

$$N_{b4}=\frac{1}{L^3}[({}^1\hat{x}_1)^3L-2({}^1\hat{x}_1)^2L^2) \tag{5.4b}$$

where $l$ is the length of frame element in the configuration at time $t$. In eqn (5.3), $\hat{u}_i$, $\hat{v}_i$, and $\hat{\theta}_i$ $(i=1, 2)$, are, respectively, the axial nodal displacements, the bending nodal displacements, and nodal rotations at nodes $i$. Since for the frame element the only stress is the normal stress on its cross-sectional area, we only consider the corresponding longitudinal strain. The normal strain for any point of the cross section of the member in the configuration at time $t$ is written as

$$\hat{e}=\hat{e}_r+\hat{e}_b=\frac{d_1^2\hat{u}}{d^1\hat{X}_1}-t\frac{d^2({}^1\hat{v})}{d({}^1\hat{X}_1)^2} \tag{5.5}$$

where $\hat{e}_r$ and $\hat{e}_b$ are, respectively, the axial and bending strain in the body attached coordinate system and $t$ is the distance from the axis of centroid to the measured point on the cross section.

For the analysis of plane solids, a four-node plane stress element as shown in Figure 5.2 is considered. The coordinate of the four-node plane stress element in the configuration at time $t$ are determined by

$${}^1X_1=\sum_{k=1}^{4}N_k\,{}^1X_1^k,\quad {}^1X_2=\sum_{k=1}^{4}N_k\,{}^1X_2^k \tag{5.6}$$

where the interpolation functions $N_k(r, s)$ are given by

$$N_1=\frac{1}{4}(1-r)(1-s),\quad N_2=\frac{1}{4}(1+r)(1-s)$$

$$N_3=\frac{1}{4}(1+r)(1+s),\quad N_4=\frac{1}{4}(1-r)(1+s)$$

Since we use isoparametric finite element discretization, the element displacements are interpolated in the same way as the geometry, i.e.,

$${}^2u_1=\sum_{k=1}^{4}N_k\,{}^2u_1^k,\quad {}^2u_2=\sum_{k=2}^{4}N_k\,{}^2u_2^k \tag{5.8}$$

where ${}^2u_1^k$, $(k=1, 2, 3, 4, i=1, 2)$, are the nodal displacements along the directions $i$ in the confi-

guration at time $t$. The element stiffness matrix in the configuration at time $t$ is now constructed by evaluating the strain-displacement matrix ${}^{1}\underline{B}$. By considering the linear part of Green-Lagrange strain tensor ${}^{2}_{t}\underline{e}$ (eqn 2.9), the ${}^{1}\underline{B}$ is evaluated from

$$ {}^{2}_{t}\underline{e} = {}^{1}\underline{B}\,{}^{2}_{t}\underline{u} \tag{5.9} $$

where ${}^{2}_{t}\underline{u}$ is the element nodal displacement vector.

Since ${}^{1}\underline{B}$ matrix is a function of $r$ and $s$ in the isoparametric finite element formulation, we must integrate the equations of the element stiffness matrix ${}^{1}\underline{K}$ (eqn 3.4b) with respect to $r$ and $s$. Using the general type of transformation of variables and regions from Cartesian to natural coordinates, the equation for the element stiffness matrix of plane solid with thickness $t$ is written by

$$ {}^{1}\underline{K} = \int_{-1}^{1}\int_{-1}^{1} {}^{1}\underline{B}^{T}\,{}^{t}\underline{C}\,{}^{1}\underline{B}\,|J|t\,dr\,ds \tag{5.10} $$

where $|J|$ is the determinant of *Jacobian J*. For the evaluation of ${}^{1}\underline{K}$ in eqn (5.10), numerical integration scheme with four-point Gaussian quadrature is employed.

### 5.1 Cantilever beam with end forces

The large deformation behaviors of a cantilever beam with end forces shown in Figures 5.3 is studied. To this end, two loading conditions are considered: case one considered a vertical non-conservative force $P_v$ of 8 *KN* and case two considered a horizontal force $P_h$ of 30000 *KN*. The beam is modeled by five equal elements. The results are shown in Figure 5.4 and 5.5.

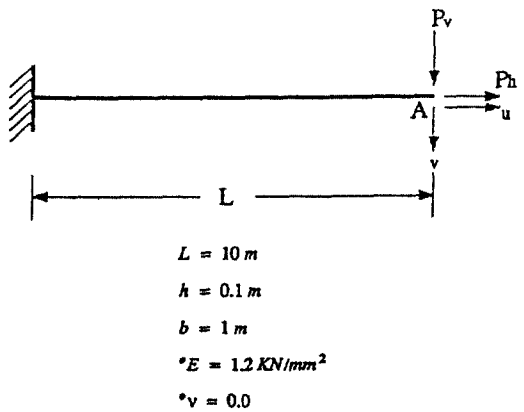


Figure 5.3. Cantilever beam with concentrated end forces.

Figure 5.4 shows good agreement between the solutions of the present study and Reference[16] and shows that the explicit solutions are very stable and converges rapidly as the number of increment loading steps increase. However, the solution obtained by ANSYS with tolerance of |0.01| and incremental load of 0.25 *KN* failed to yield converged results at $F$=3.25 *KN*. Converged results by ANSYS are only plotted in this Figure.

In Figure 5.5, the results are compared to those by ANSYS. Incidentally, the result by ANSYS with large displacement analysis is the same as the result by linear analysis for the second loading case. In a practical sense, since the stiffness of beam element becomes softer when it is elongated, the axial displacement should be larger in large deformation analysis than in linear analysis, if the same material properties and the same are used. Another plots using ${}^{t}E$ is alos shown for a comparison. From the Figure, we see that stiffness of the cantilever beam becomes bigger as the beam becomes elongated.

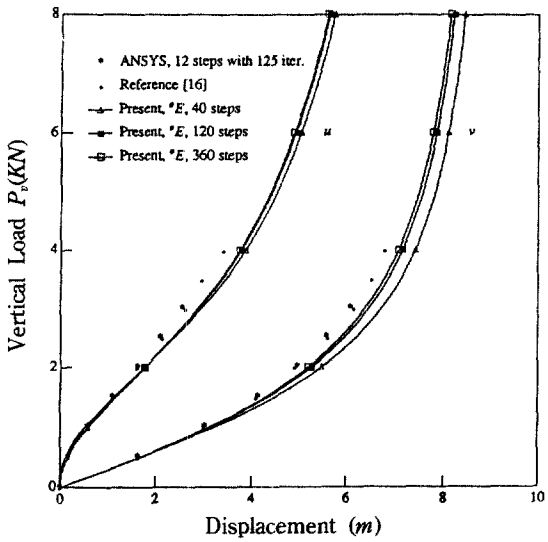


Figure 5.4. Horizontal and vertical displacements of a cantilever beam with a concentrated load $P_v$.

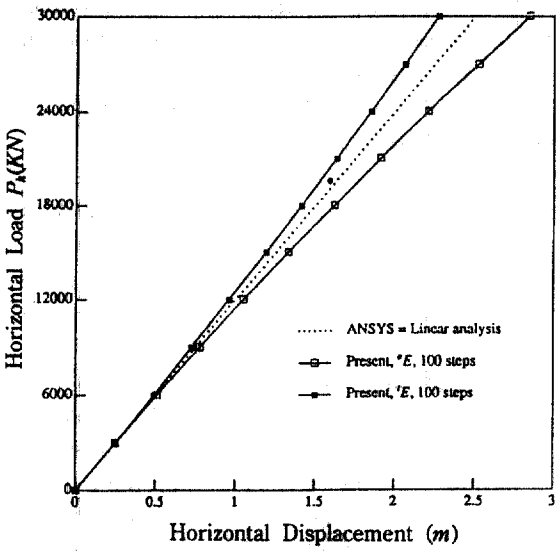


Figure 5.5. Horizontal displacement of a cantilever beam subjected to a concentrated load $P_h$.

### 5.2 Cantilever beam with an end moment

A cantilever beam subjected to a concentrated moment $M$ at the free end as shown in Figure 5.6 is considered. This beam is modeled by twelve equal elements. The results are shown in Figures 5.7 and 5.8.

Figure 5.7 shows the plot of normalized displacements versus load factor $f$ for the tip of the beam. results are compared with those of Reference [17]. In Reference[17]. total Lagrangian approach with incremental iterations is used to handle geometrically nonlinear three dimensional beam problems. The results show that the predicted response compares well with those of reference [17].

Figure 5.8 shows the deformed shapes of the cantilever beam obtained by the presented method for the maximum load of $f=1.8$ with 90 incremental load steps and $f=3.6$ with 180 incremental load steps. From the deformed shapes of the beam, we may see the differences of the results by $^oE$ and $^tE$ and the capabilities of handling large displacement and large rotation problems.

### 5.3 Diamond-shaped frame

A diamond-shaped frame composed of four

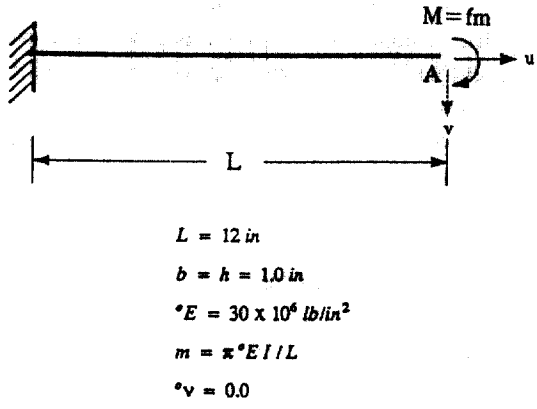


Figure 5.6. Cantilever beam with an end moment.

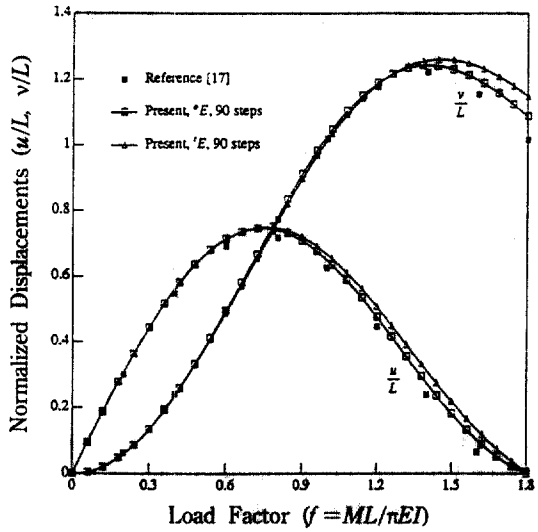


Figure 5.7. Load-displacement curves of a cantilever beam sugjected to an end moment $M$.

equal bars and loaded by forces applied at a pair of diagonally opposite joints as shown in Figure 5.9 is analyzed. The two loaded joints are assumed to be hinged while the two free joints are assumed to be rigid. A quarter of the frame is modeled by ten equal elements. The results are shown in Figures 5.10 an 5.11.

Figures 5.10 and 5.11 show the plot of normalized displacements versus load factors under tensile and compressive loadings. Results are compared with those of Reference [18] where analytical solutions with experimental results for this frame

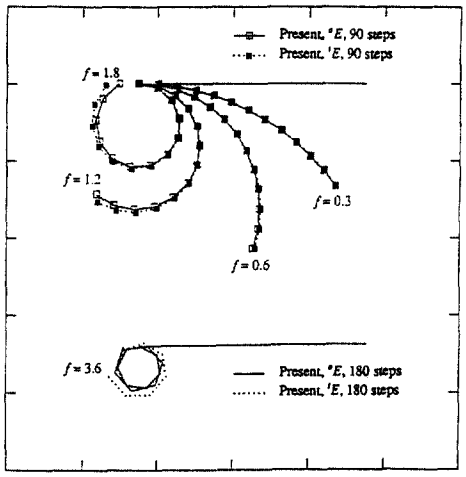


Figure 5.8. Deformed shapes of cantilever beam.

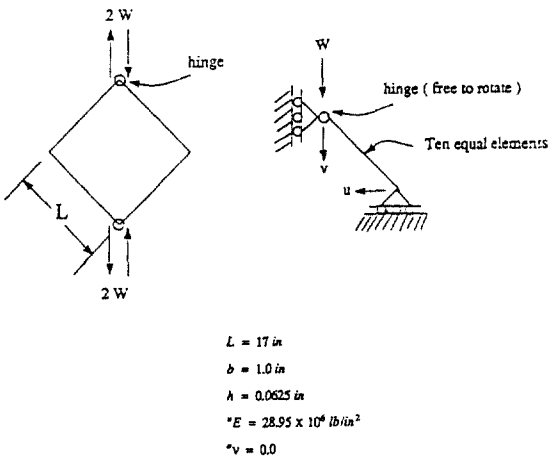


Figure 5.9. Diamond-shaped frame structure.

are provided. The solutions from the figures show excellent agreement with theory[18].

### 5.4 Plane solid subjected to concentrated nodal forces

The plane solid which is composed of 15 equal-size elements and subjected to four equal concentrated forces with fixed ends shown in Figure 5.12 is considered. The problem has also been solved by using ANSYS. ANSYS failed to yield converged results at $F=820(lb)$ with a large tolerance of |0.01|. Using the simple incremental procedure with

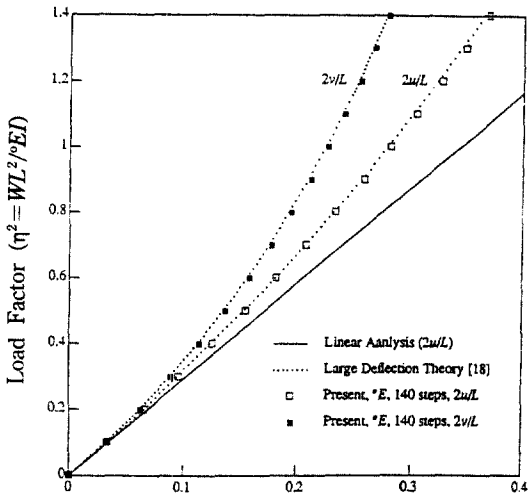


Figure 5.10. Vertical and horizontal displacements of a pinned-fixed frame under tensile loading.

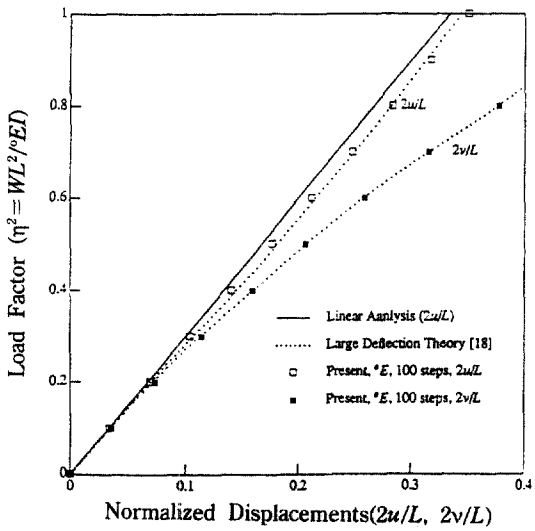


Figure 5.11. Vertical and horizontal displacements of a pinned-fixed frame under compressive loading.

increment force of $\Delta F=50(lb)$, the solutions by ANSYS became very unstable at $F=1550(lb)$. The present algorithm appears to have no such limit. Figures 5.13 and 5.14 show the comparisons of the load-displacement relationships. From the figures, we see that the solutions are very stable and the algorithm has the capability of following very large deformations of the structure.

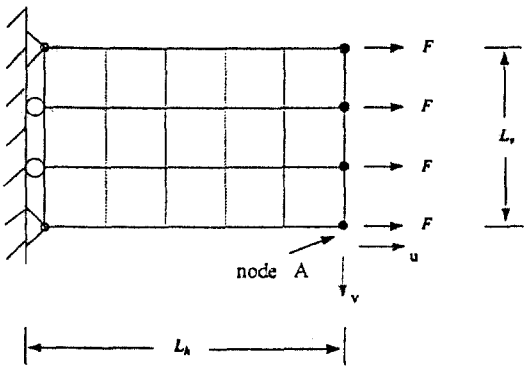


$L_h$ = 15 *in*

$L_v$ = 9 *in*

*thickness* = 1.0 *in*

*E = 1.2 x $10^3$ *lb/in*$^2$

*ν = 0.33

Figure 5.12. Plane solid subjected to horizontal nodal forces.

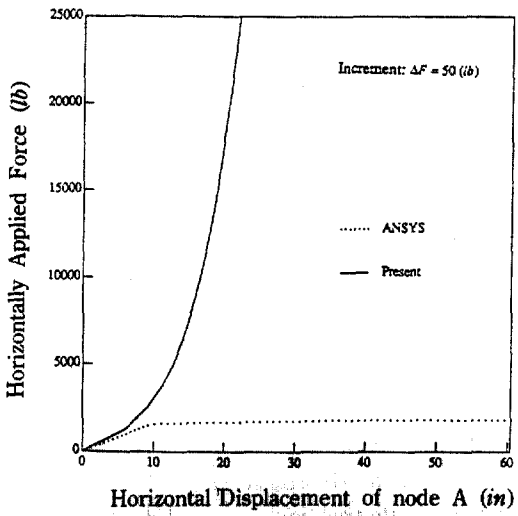


Figure 5.13. Horizontal displacement of node *A* of plane solid subjected to horizontal loads.

## 6. Conclusion

The objective of this paper was to develop a nonlinear finite element formulation which has the capability of handling very large geometrical changes. The formulation was based on an updated material reference frame and hence true stress-

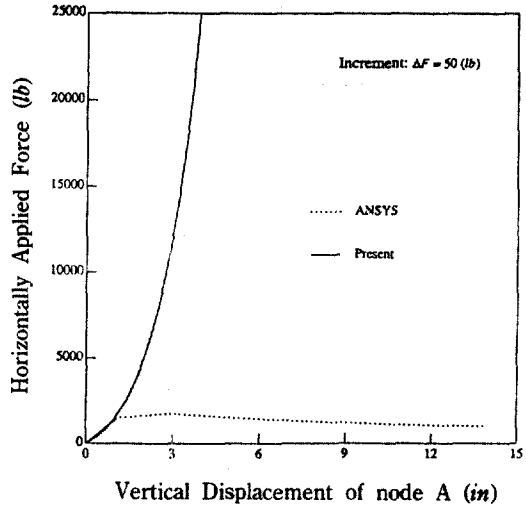


Figure 5.14. Vertical displacement of node *A* of plane solid subjected to horizontal loads.

strain test can be directly applied to properly characterize properties of materials which are subjected to very large deformation. For the large deformation, a consistent formulation based on the continuum mechanics approach has been derived. The kinematics has been referred to an updated material frame. Body equilibrium has also been established in an updated geometry and the second Piola-Kirchhoff stress and the updated Lagrangian strain tensor have been used in the formulation.

From the example considered, we see that the present formulation has the capability of handling very large geometrical changes. In addition the algorithm, incremental numerical procedure developed here, has shown to be very stable and converges rapidly when small load or deformation increments are used. The importance of using proper material properties has been demonstrated from the differences of results.

## Reference

1. J.T. Oden, *Finite Elements of Nonlinear Continua.* McGraw-Hill, New York (1972).
2. K.J. Bathe and E. Ramm and E.L. Wilson, Finite element formulations for large deformation dyna-

mic analysis. *Int. J. Num. Meth. Engng.*, **9**, 353-386(1975).

3. F. Frey and S. Cescotto, Some new aspects of the incremental total Langrangian description in nonlinear analysis. *Proc. Int. Conf. Finite Elements in Nonlinear-Solids and Structural Mechanics* (Edited by P. Pergan et al.) 323-343. Geilo (1977) Tapir Publishers, Univ. of Trondheim (1978).
4. M.S. Gadala, G.AE. Oravas and M.A. Dokainish, Continuum bases and consistent numerical formulations of nonlinar continuum mechanics problems. *Solid Mechanics Archive,* 9, 1-52 (1984).
5. H.D. Hibbit, P.V. Marcal and J.R. Rice, A finite element formulation for problems of large strain and large displacements. *Int. J. Solids Struct.*, 6, 1069-1086 (1970).
6. W. Wunderich, Incremental formulations for geometrically nonlinear problems. In *Formulations and Computational Algorithms in Finite Element Analysis: U.S.-Germany Symp.* (Edited by K.J. Bathe et al.), pp. 193-240 (1976).
7. M. Hartzman and J.R. Hutchinson, Nonlinear dynamics of solids by the finite element method. *Comput. Structures,* 2, 47-77 (1972).
8. S. Nemat-Nasser and H.D. Shattoff, A consistent numerical method for the solution of nonlinear elasticity problems at finite strains. *SIAM J. Appl. Math.* 20, 462-481 (1971).
9. S.W. Key, A finite element procedure for the large deformation dynamic reponse of axisymmetric solid. *Comp. Meth. Appl. Engng.*, 4, 195-218 (1974).
10. D.W. Murray and E.L. Wilson, Finite-element large deflection analysis of plates. *J. Engng. Mech. Div., ASCE Proc.* 95, 143-165 (1969).
11. S. Yaghmai and E.P. Popov, Incremental analysis of large deflections of shells of revolution. *Int. J. Solids Struct.*, 7, 1375-1393 (1971).
12. Y. Yamada, Constitive modelling of inelastic behavior and numerical solution of nonlinear problems by the finite element method. *Comput. Structures,* 8, 533-543 (1978).
13. J.H. Argyris, J. St. Doltsinis and M. Kleiber, Incremental formulation nonlinear mechanics and large strain elasto-plasticity-natural approach-II, *Comp. Meth. Appl. Mech. Engng.*, **14**, 259-294 (1978).
14. W. Kanok-Nukulchai, A. Hasegawa and F. Nishino, Generic formulation procedure for large deformation analysis of structural element. *Proc. of JSCE, No.* 368/1-5, 53s-61s (1986).
15. W. Kanol-Nukulchai and W.K. Wong, Element-based Lagrangian formulation for large-deformation analysis. *Comput. Structures,* **30**, 967-974 (1988).
16. G. Horrigmore and P.G. Bergan, Nonlinear analysis of free-from shells by flat finite elements. *Comput. Meth. Appl. Mech. Engng.*, **16**, 11-35 (1978).
17. K.S. Surana and R.M. Sorem, Geometrically nonlinear formulation for three dimensional curved beam elements with large rotations., *Int. J. Num. Meth. Engng.*, **28**, 43-73 (1989).
18. J.A. Jenkins, T.B. Seitz and J.S. Przemieniecki, Large deflections of diamond shaped frames., *Int. J. Solids Struct.*, **2**, 591-603 (1966).

(接受：1992. 5. 22)